

Novel Double-Chirp Preamble Design for Multiuser Asynchronous Massive MIMO LoRa Networks

The Khai Nguyen and Ebrahim Bedeer

Abstract—This paper proposes a novel preamble design and detection method for multiuser asynchronous massive MIMO LoRa networks. Unlike existing works, which only consider the preamble detection for a single target end devices (ED), we proposed to simultaneously detect the preambles of multiple EDs that asynchronously transmit their uplink (UL) packets to a multiple-antenna gateway (GW). First we show that the preamble detection in multiuser LoRa networks with the conventional *single-chirp* preamble suffers from the so-called *preamble resemblance* effect. This means that the preamble of any single ED can resemble the preambles of all EDs in the network, and make it impossible to determine to which ED a preamble belongs. To address this problem, a novel *double-chirp* preamble design and a preamble assignment method are proposed, which can mitigate the *preamble resemblance* effect by making the preamble of each ED unique and recognizable. Next, a maximum-likelihood (ML) based detection scheme for the proposed *double-chirp* preamble is derived. Finally, since the proposed algorithm requires the calculation of the discrete Fourier transform (DFT) every sampling period, we proposed a low-complexity technique to calculate the DFT recursively to reduce the complexity of our proposed design. Simulation shows that the proposed preamble detection design and detection requires just about 2 dB more power to increase the number of EDs from one to 15 in the Rayleigh fading channel while achieving the same preamble detection error performance.

Index Terms—LoRaWAN, massive MIMO, multiuser preamble detection.

I. INTRODUCTION

LoRaWAN is a standard for low-power wide-area networks that has been well received as a key technology for Internet of Things (IoT) [1], [2]. In the physical layer, LoRa adopts the chirp spread spectrum (CSS) modulation, also known as the LoRa modulation. The CSS signal has linearly-varying frequency and constant signal envelops, which can provide the robustness against Doppler shift, and can offer very long-range, lower-power communication, yet can be implemented efficiently with the simple discrete Fourier transform (DFT) based receiver. In the medium access control (MAC) layer, LoRa uses pure ALOHA protocol, which, despite having low complexity, has a high risk of packet collision when end devices (EDs) operate with the same spreading factors (SFs). Thus, LoRa often resorts to a duty cycle limit to avoid collisions. This results in a bottleneck in both the capacity and connectivity of LoRaWAN in environments with high ED density, which is the current and future scenarios of modern IoT networks. Solving this problem to enable concurrent transmission-reception in LoRaWAN requires the solutions of three subproblems: preamble detection, channel estimation and multiuser detection.

The authors are with the Department of Electrical and Computer Engineering, University of Saskatchewan, Saskatoon, Canada S7N5A9. Emails: {khai.nguyen, e.bedeer}@usask.ca.

In terms of multiuser detection, to deal with packet collisions in LoRaWAN, the works in [3]–[6] utilize successive interference cancellation (SIC) to detect collided packets from different EDs. The payload of the EDs is decoded in a successive manner, and then subtracted before detecting the payloads of the succeeding packets. In [7], the time-frequency offsets and power characteristics of different LoRa packets are exploited to develop a maximum likelihood (ML) detector for the case of two EDs. In [9], a non-coherent detector for multiuser GW massive MIMO LoRa systems is studied. The cooperative GWs differentiate EDs based on their distinctive relative locations from the GWs and the unique received power signatures. In [10], [11], multiuser LoRa reception is realized with coherent detection, which take advantage of the asymptotic orthogonality among channels of different EDs. In [12], the authors proposed listen-before-talk protocols to reduce collision in LoRaWAN. The scheme is developed for both the physical and MAC layer, which demonstrates collision reduction performance by sacrificing complexity and transmit power.

Most of the aforementioned works [3]–[5], [7], [10] requires channel state information (CSI), which means extra overhead for pilot training. To address this overhead, in [13], [14], the authors propose a semi-coherent detection method. The channel is estimated iteratively based on the detected data, which does not require any overhead associated with pilot training. In [10], [11], [15], channel estimation methods based on preambles for multiuser LoRa networks are presented. However, one critical requirement for the methods in [10], [15] is that signals from different EDs must be *synchronized* at packet level (i.e., preambles from all EDs must be aligned), which indicates that slotted ALOHA is required. Whereas, the method in [11] can work even with pure ALOHA with asynchronous packets.

In order to realize multiuser detection and channel estimation in LoRaWAN, preamble detection is the first step and hence, is of highest importance. However, this topic has not received adequate attention in the literature, and mostly considers single-ED preamble detection. The majority of existing works in LoRa preamble detection is based on *majority vote* [16]–[19]. First the signal is processed with the conventional discrete Fourier transform (DFT) based receiver. Then, the power of the signal in the frequency domain is compared with a preset threshold to detect the presence of the preamble. If the threshold is surpassed at the same frequency bin multiple times over multiple consecutive DFT blocks, the GW determines that a preamble is present. The condition for the number of power peaks that surpass the threshold to a preamble can vary. Experimentally, at least 4 consecutive peaks on the same frequency bin must surpass the threshold to

declare the presence of a preamble [17]. In [17], the authors propose to relax this condition such that the peaks are not required to be consecutive, but must still remain within the preamble length. The relaxed condition results in a lower probability that the GW misses the presence of a preamble. In [16], the authors propose to count the peaks that surpass the threshold on multiple adjacent bins rather than just one single bin as conventional. This modification accounts for the Doppler effect that causes undesirably frequency offset to the bins in the DFT domain, and results in an improved performance. In [18], [19], the peaks are obtained by averaging the power of multiple consecutive DFT blocks to obtain a better performance at low SNR. However, both the threshold value and the number of peaks are not optimized, but rather chosen arbitrarily, which leads to a strict suboptimal performance [20].

To improve the preamble detection performance, in [20], [21], the authors proposed preamble detection methods that consider the effect of noise and interference to find optimal thresholds for preamble detection. Unlike previous works that only focus on the aspect of maximizing the preamble detection rate, the work in [20] also takes into account the effect of false alarm, which can have a much more negative impact on the performance of LoRaWAN. In [22], the author extended the work in [20] for fading channel with both coherent and non-coherent detection. A closed-form expression for the threshold was derived, which leads to a significantly better performance compared to previous works. In [23], a detail study of LoRa preamble detection based on the hypothesis model in [20] is performed under the consideration of timing and frequency offset, which results in a more robust and complete design. In [24], the design for LoRa synchronization and start-of-frame detection is investigated. The properties of the transmitted and received preamble signal are studied, which results in an algorithm that can simultaneously perform carrier frequency-offset, time-offset, and start-of-frame recovery.

Although some of the aforementioned works did take the effect of *inter-user interference* into account, only the preamble detection for a single target ED is considered. Moreover, the interference caused by data payloads and preambles are generalized as a common *inter-user interference* and thus, oversimplified. To the best of our knowledge, the effect of interfering preambles to the preamble of a different ED has not been sufficiently investigated. In LoRaWAN, where multiple EDs concurrently transmit on the same time-frequency resources, using the same spreading factor (SF), even if a preamble is successfully detected, it is impossible to determine to which ED that preamble belongs. In this paper, we will show that the culprit is the so-called *preamble resemblance* effect. This means that a conventional LoRa preamble of any ED can resemble the preambles of any other EDs. Consequently, the GW cannot determine the identity of the detected ED only based on the information in the preamble.

Therefore, in this paper, we propose a novel preamble design that enables the multiuser preamble detection, with the aid of a massive MIMO GW. The proposed design uses *double-chirp* preambles, which means that a preamble is the sum of two different chirps, that are uniquely assigned to only one ED in the network. The proposed double-chirp

preamble is designed and assigned in a way such that preamble resemblance can be avoided. Whereas, the massive MIMO GW provides the asymptotic orthogonality among the channels of different EDs to the GW [25], which provides the robustness against noise and interference in preamble detection. A ML-based non-coherent preamble detection algorithm is then derived to simultaneously detect the preamble of multiple EDs. Next, since the proposed algorithm requires the calculation of the DFT every sampling period, we proposed a recursive technique to replace the fast Fourier transform (FFT) used in the DFT-based LoRa receiver. The proposed technique can reduce the complexity of calculating the DFT in our proposed technique by order of the SF.

The remainder of this paper is organized as follows. Section II presents the multiuser LoRa system model and reviews fundamental background on LoRa modulation, demodulation and preamble detection. Section III introduces the novel double-chirp preamble design and analyzes the *preamble resemblance* effect. Section IV derives the ML-based preamble detector. Section V analyzes the complexity of the proposed double-chirp preamble ML-based detection, and proposes a complexity reduction method for the proposed design. Finally, Section VI provides simulation results, and Section VII concludes the paper.

Notations: The following notations are used throughout the paper. Transpose matrices are denoted by $[\cdot]^T$. Hermitian matrices are denoted by $[\cdot]^H$. The averaging (expectation) of a random variable or random vector is denoted by $\mathbb{E}\{\cdot\}$. The norm of a vector is denoted by $\|\cdot\|$. The real and imaginary parts of a complex number are denoted by $\Re\{\cdot\}$ and $\Im\{\cdot\}$, respectively. The modulo operator is denoted by mod . The set of $d_1 \times d_2$ complex matrices is denoted by $\mathbb{C}^{d_1 \times d_2}$. The complex normal distribution with variance σ^2 is denoted by $\mathcal{CN}(0, \sigma^2)$. The complex conjugate is denoted by $(\cdot)^*$. The determinant of a squared matrix is $\det(\cdot)$. The pairwise multiplication is denoted by \otimes . Circular shift operations of a vector \mathbf{a} by b elements to the left and the right are denoted by $\mathbf{a} \ll b$ and $\mathbf{a} \gg b$, respectively.

II. MULTIUSER LORAWAN SYSTEM MODEL AND CHALLENGES WITH CONVENTIONAL PREAMBLE DESIGN

This section introduces the multiuser LoRa system model and reviews the fundamentals of LoRa detection with the DFT-based receiver, conventional LoRa preamble structure and its challenges when being implemented in a multiuser scenario.

A. System model

Consider a LoRa network where N_u single-antenna EDs simultaneously transmit uplink (UL) packets to a GW with L antennas. With pure ALOHA, the packets from different EDs are asynchronous. Each LoRa packet has multiple symbols, which are drawn from a set of $M = 2^{\text{SF}}$ linearly-frequency-variant LoRa symbols (also known as chirps). Specifically, the \tilde{m} th chirp is defined as $\mathbf{s}_{\tilde{m}} = [s_{\tilde{m},1}, s_{\tilde{m},2}, \dots, s_{\tilde{m},M}]^T$, where $\tilde{m} = 0, 1, \dots, M-1$. The 0th chirp is known as the basic upchirp, whose samples are defined as:

$$s_{0,m} = \exp \left\{ j2\pi \left(\frac{(m-1)^2}{2M} - \frac{m-1}{2} \right) \right\}. \quad (1)$$

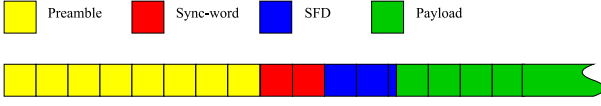


Fig. 1: LoRa packet structure.

Then, the m th sample of the \tilde{m} th chirp can be obtained from $s_{0,m}$ as $s_{\tilde{m},m} = s_{0,m+\tilde{m}}$. From this chirp set, a LoRa packet is constructed with the structure in Fig. 1, which starts with N consecutive identical basic upchirps s_0 called the *preamble*, followed by 2 symbols known as *sync-words* (used for network identifier), then 2.25 basic downchirp s_0^* of *start-frame delimiter (SFD)* marking the beginning of the data.

Since each LoRa symbol consists of M discrete samples, the detection of each LoRa symbol must be performed collectively on M consecutive samples in the time domain. Let $\mathbf{Y}_n = [\mathbf{y}_{n,1}, \mathbf{y}_{n,2} \dots \mathbf{y}_{n,L}]^\top \in \mathbb{C}^{L \times M}$ be the signal received on L antennas at the GW during one LoRa symbol period from the discrete time n to $n + M - 1$, where $\mathbf{y}_{n,\ell} = [\mathbf{y}_{n,\ell}, \mathbf{y}_{n+1,\ell} \dots \mathbf{y}_{n+M-1,\ell}]^\top \in \mathbb{C}^{M \times 1}$, is the received signal on the ℓ th antennas from the discrete time n to $n + M - 1$. Consider Rayleigh fading channel, \mathbf{Y}_n can be expressed as:

$$\mathbf{Y}_n = \sum_{u=1}^{N_u} \mathbf{h}_u \bar{\mathbf{x}}_{n,u}^\top + \boldsymbol{\Omega}_n, \quad (2)$$

where $\mathbf{h}_u \sim \mathcal{CN}(0, \mathbf{I}_L)$ denotes the uncorrelated Rayleigh fading channel from the u th ED to the GW (\mathbf{I}_L is the identity matrix of size L), $\bar{\mathbf{x}}_{n,u} \in \mathbb{C}^{M \times 1}$ is the M -sample signal vector of the u th ED during one LoRa symbol period, and $\boldsymbol{\Omega}_n \in \mathbb{C}^{L \times M}$ is the AWGN noise matrix with i.i.d. elements $\omega_{\ell,m} \sim \mathcal{CN}(0, \sigma^2)$. Note that the signal from each ED $\bar{\mathbf{x}}_{n,u} \in \mathbb{C}^{M \times 1}$ can be partially or completely preamble and/or payload. This is due to the asynchronous nature of ALOHA at MAC layer, where packets transmitted from different EDs are not necessarily synchronized.

B. LoRa data and preamble detection in single-ED scenario

The most common LoRa modulation method is the DFT-based receiver, which can be performed on the signal $\mathbf{y}_{n,\ell}$ separately on each and every antenna. First, $\mathbf{y}_{n,\ell}$ is dechirped with the conjugate of the basic chirp s_0 , then transformed with the DFT to obtain the power distribution on M frequency bins as $\mathbf{V}_{n,\ell} = [V_{n,\ell}[0], V_{n,\ell}[1] \dots V_{n,\ell}[M-1]]^\top$:

$$\mathbf{V}_{n,\ell} = \text{DFT}\{\mathbf{y}_{n,\ell} \otimes s_0^*\} \in \mathbb{C}^{M \times 1}. \quad (3)$$

Suppose only the u th ED is transmitting, if the signal $\mathbf{y}_{n,\ell}$ received on the ℓ th antenna is perfectly synchronized with a transmitted LoRa chirp, say $s_{\tilde{m}}$, all of the chirp power will be focused on the \tilde{m} th bin, while the remaining bins receive zero power from that chirp [13]. Mathematically, suppose:

$$\mathbf{y}_{n,\ell} = \mathbf{h}_{u,\ell} s_{\tilde{m}} + \boldsymbol{\omega}_{n,\ell}, \quad (4)$$

where $\mathbf{h}_{u,\ell}$ is the channel from the u th ED to the GW on the ℓ th antenna (the ℓ th element of \mathbf{h}_u), and $\boldsymbol{\omega}_{n,\ell}$ is the AWGN noise sample vector on the ℓ th antennas from time n to $n + M - 1$

(the ℓ th row of $\boldsymbol{\Omega}_n^\top$). When performing the dechirping, the dechirped LoRa chirp component $s_{\tilde{m}} \otimes s_0^*$ becomes:

$$\begin{aligned} s_{\tilde{m},m} s_{0,m}^* &= \exp \left\{ j2\pi \left(\frac{(m+\tilde{m}-1)^2}{2M} - \frac{m+\tilde{m}-1}{2} \right) \right\} \\ &\times \exp \left\{ -j2\pi \left(\frac{(m-1)^2}{2M} - \frac{m-1}{2} \right) \right\} \\ &= \underbrace{\exp \left\{ j2\pi \left(\frac{\tilde{m}^2}{2M} - \frac{\tilde{m}}{2} \right) \right\}}_{\text{constant phase } \theta_{\tilde{m}}} \underbrace{\exp \left\{ j2\pi \tilde{m}(m-1) \right\}}_{\text{linear phase}}. \end{aligned} \quad (5)$$

As can be seen, the quadratic phase component of the LoRa chirp $s_{\tilde{m}}$ has been eliminated by dechirping, and only the linear phase component remains with the discrete frequency of \tilde{m} . Consequently, as can be seen in Fig. 2-(a), when DFT is performed on the dechirped signal $\mathbf{y}_{n,\ell} \otimes s_0^*$, all the power of the chirp $s_{\tilde{m}}$ is focused on the \tilde{m} th bin:

$$V_{n,\ell}[k] = \begin{cases} \sqrt{M} h_{u,\ell} \exp(j\psi_{\tilde{m}}) + W_{n,\ell}[k], & k = \tilde{m} \\ W_{n,\ell}[k], & \text{otherwise,} \end{cases} \quad (6)$$

where $\mathbf{W}_{n,\ell} = [W_{n,\ell}[0], W_{n,\ell}[1] \dots W_{n,\ell}[M-1]]^\top = \text{DFT}\{\boldsymbol{\omega}_{n,\ell}\}$, and $\theta_{\tilde{m}} = 2\pi \left(\frac{\tilde{m}^2}{2M} - \frac{\tilde{m}}{2} \right)$ is a deterministic bin-dependent phase offset, which can be conveniently discarded by converting $V_{n,\ell}[k]$ into:

$$\tilde{V}_{n,\ell}[k] = \frac{V_{n,\ell}[k]}{\exp(j\theta_{\tilde{m}})} = \begin{cases} \sqrt{M} h_{u,\ell} + \tilde{W}_{n,\ell}[k], & k = \tilde{m} \\ \tilde{W}_{n,\ell}[k], & \text{otherwise.} \end{cases} \quad (7)$$

Thus, when there is only one ED is transmitting, once the preamble detection and synchronization are finished, the demodulation can be done with squared-law combining [13], in other words, by simply calculating the power of all M frequency bins gathered from all L antennas $\mathbf{\Upsilon}_n = [\Upsilon_n[0], \Upsilon_n[1] \dots \Upsilon_n[M-1]]^\top$, where:

$$\Upsilon_n[k] = \sum_{\ell=1}^L \left| \tilde{V}_{n,\ell}[k] \right|^2. \quad (8)$$

The bin with the highest power is the one corresponding to the transmitted LoRa symbol.

Whereas, if $\mathbf{y}_{n,\ell}$ is not synchronized with a LoRa symbol, but overlapped between two consecutive LoRa symbols s_{m_1} and s_{m_2} , such that $\mathbf{y}_{n,\ell} = \mathbf{h}_{u,\ell} \bar{\mathbf{s}}$, where

$$\bar{\mathbf{s}} = \underbrace{[s_{m_1,\tau+1}, s_{m_1,\tau+2} \dots s_{m_1,M}, s_{m_2,1}, s_{m_2,2} \dots s_{m_2,\tau}]}_{\text{tail of } s_{m_1}} \underbrace{[s_{m_2,\tau+1}, s_{m_2,\tau+2} \dots s_{m_2,M}]}_{\text{head of } s_{m_2}}, \quad (9)$$

with $\tau < M$. When $\bar{\mathbf{s}}$ is dechirped by multiplying with s_0^* , following (5), the signal $\bar{\mathbf{s}} \otimes s_0^*$ has the m th elements as:

$$\begin{aligned} \bar{s}_m s_{0,m}^* &= \begin{cases} s_{m_1,\tau+m} s_{0,m}^*, & m \leq M-\tau \\ s_{m_2,m-(M-\tau)} s_{0,m}^*, & m > M-\tau \end{cases} \\ &= \begin{cases} \exp\{j\theta_{\tilde{m}_1}\} \exp\left\{ \frac{j2\pi \tilde{m}_1(m-1)}{M} \right\}, & m \leq M-\tau \\ \exp\{j\theta_{\tilde{m}_2}\} \exp\left\{ \frac{j2\pi \tilde{m}_2(m-1)}{M} \right\}, & m > M-\tau. \end{cases} \end{aligned} \quad (10)$$

where $\tilde{m}_1 = m_1 - \tau$ and $\tilde{m}_2 = m_2 + M - \tau$. The dechirped signal now contains the fragments of two discrete sinusoids

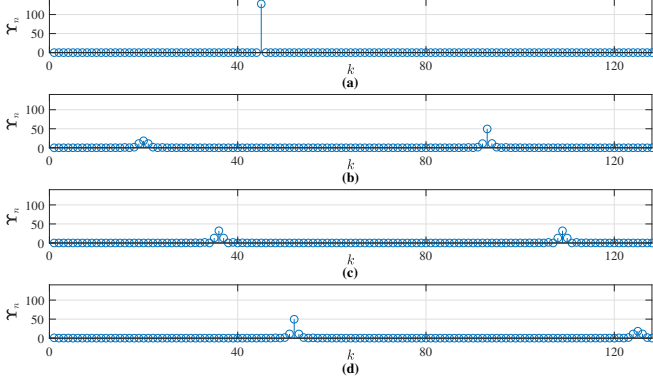


Fig. 2: DFT output of the dechirped window with s_{44} and s_{99} (SF = 7). (a) $\tau = 0$, (b) $\tau = 48$, (c) $\tau = 64$, (d) $\tau = 80$.

with two different frequencies. As a result, the power in the two fragments from two consecutive LoRa symbols is spread unevenly over M frequency bins, focused around the two frequencies \tilde{m}_1 and \tilde{m}_2 in the frequency domain as illustrated in Fig. 2-(b), (c) and (d) with different values of τ . This highlights the importance of detecting the LoRa preamble and synchronization.

Next, we review the preamble detection of the conventional LoRa to detect the preamble of a single ED at a time. Since a LoRa symbol is M samples in length, to detect the preamble, the GW uses a window spanning over M samples in the time-domain as shown in Fig. 3. In [16]–[19], the window slides along the time-domain, one *symbol* at a time, which has a low complexity. Another equivalent way is to shift the window by one *sample* at a time. Although with this way, the complexity is higher since the signal processing must be performed every sample, rather than every symbol (M samples), we chose to discuss the conventional preamble detection in this way since it is similar to the signal processing in our proposed design. The higher complexity issue (as compared to shifting the window every symbol) will be addressed in Section V. Conventionally, the LoRa preamble is made of $N = 8$ consecutive basic upchirps (s_0). To detect these N consecutive basic upchirps, the GW observes the power of the frequency bins in the frequency domain as in (8). Since the preamble is N consecutive basic upchirps, the GW specifically observes the 0th frequency bin $\Upsilon_n[0]$ over time to find $N = 8$ consecutive power peaks, separated by M samples (or 1 LoRa symbol time) as shown in Fig. 4-a. To differentiate this with peak samples caused by noise or interference, we specifically refer to the consecutive peaks associated with the N identical symbols of the preamble as *preamble peaks* (PPs). Thus, when the GW observes N consecutive basic upchirps, or in other words, N consecutive PP on $\Upsilon_n[0]$, it decides that a preamble is present, and a new packet is coming. Then, the GW synchronizes the reception to the time instance of the first detected peak with the aid of the SFD field [24].

C. Challenges with conventional single-chirp preamble in multiuser LoRa

In multiuser scenario, with the conventional preamble design with N consecutive basic upchirps, once the GW detects the presence of a preamble, it is impossible to determine to

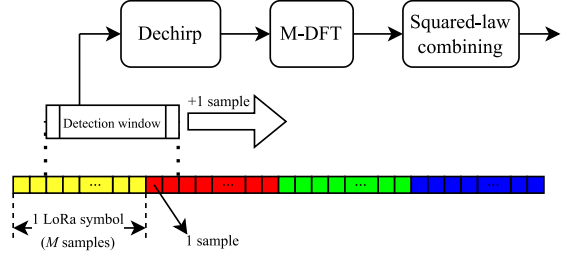


Fig. 3: Conventional single-chirp preamble detection.

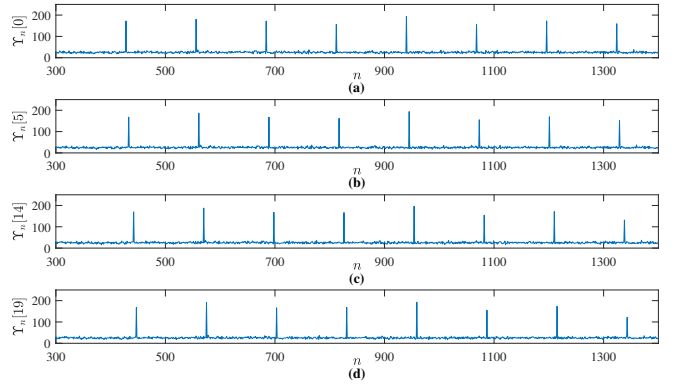


Fig. 4: DFT output of the dechirped window after squared-law combining over time (SF = 7, $L = 64$ antennas). The preamble of an ED can trigger PPs on every frequency bin.

which ED that the detected preamble belongs, based solely on the information of the preamble, since all EDs use the same preamble. Furthermore, under the influence of noise and interference among EDs, the probability that the GW fails to detect preambles is high.

One possible solution is to assign different single-chirps to different EDs to use as preambles, for example, the u th ED is assigned with the u th chirp (s_u) to use as a preamble. With this approach, although one can say that the GW only needs to observe the u th bin corresponding to the preamble of the u th ED to detect its incoming packet, this task is far from simple. This is because, with the detection window slides in the time domain to capture M consecutive samples, the preamble of the u th ED (assumed to be a repetition of the u th chirp) does not only result in N PPs in the u th bin, but it also creates N PPs in every other frequency bins. This effect is illustrated in Fig. 4, and can be explained as follows. Suppose the first preamble symbol of the u th ED (s_u) is synchronized completely into the detection window at time n , which is:

$$\mathbf{y}_{n,\ell} = h_{u,\ell} s_u + \mathbf{\omega}_{n,\ell}, \quad (11)$$

and results in a PP in the corresponding u th bin. Since the chirp s_u is repeated N times, when the detection window shifts by one sample, the signal $\mathbf{y}_{n+1,\ell}$ taken from the discrete time $n+1$ to $n+M$ will capture the last $M-1$ samples of the chirp s_u that belongs to the first symbol of the preamble, and the first sample of the second symbol of the preamble $s_{u,1}$,

which is exactly the $(u+1)$ th chirp \mathbf{s}_{u+1} . As a result:

$$\begin{aligned}\mathbf{y}_{n+1,\ell} &= h_{u,\ell}[s_{u,2}, s_{u,2}, \dots, s_{u,M}, s_{u,1}]^\top + \boldsymbol{\omega}_{n+1,\ell} \\ &= h_{u,\ell}\mathbf{s}_{u+1} + \boldsymbol{\omega}_{n+1,\ell},\end{aligned}\quad (12)$$

which results in a PP on the $(u+1)$ th bin. Similarly, it can be seen that at time $n+\tau$, there will be a PP on the $(u+\tau)$ th bin, which explains the effect illustrated in Fig. 4. Consequently, once a preamble is transmitted, every bin in the DFT domain will experience N consecutive peaks as shown in Fig. 4, where a preamble of $N = 8$ consecutive basic upchirps is transmitted. From the figure, it can be seen that the preamble triggers N PPs on not only the u th bin, but also all other bins followed that. In this case, with multiple EDs, the GW cannot determine which ED is transmitting the packet, even though every ED has its own unique preamble.

The above discussion shows that the biggest problem in preamble detection of multiuser LoRa networks is, what we named, *preamble resemblance*, which means that the preamble of an ED can undesirably resemble the preamble of others. Thus, it is important to develop a novel preamble design to address this problem in multiuser LoRa networks.

III. NOVEL DOUBLE-CHIRP PREAMBLE DESIGN FOR MULTIUSER MASSIVE MIMO LORA

In this section, a novel preamble design for multiuser massive MIMO LoRa networks is proposed. This preamble design helps to avoid preamble resemblance, which enables multiuser preamble detection in LoRa networks.

A. Novel double-chirp preamble design for multiuser massive MIMO LoRa

As shown in Fig. 4, even when all EDs are assigned with unique *single-chirp* preambles, the preamble of any ED can trigger N PPs in every frequency bin, which resembles the preambles of all others, and causes failure to the preamble detection of multiuser LoRa networks. Thus, instead of using *single-chirp* preamble, we propose to assign to each ED a *unique double-chirp* preamble. Specifically, the preamble of an arbitrary ED is the sum of two different chirps that are uniquely assigned to this ED, repeated N times. Suppose that the u th ED is assigned with two chirps $\mathbf{s}_{\kappa_{u,1}}$ and $\mathbf{s}_{\kappa_{u,2}}$ to use as preamble, then, the transmitted preamble of the u th ED is:

$$\boldsymbol{\rho}_u = \frac{1}{\sqrt{2}}(\mathbf{s}_{\kappa_{u,1}} + \mathbf{s}_{\kappa_{u,2}}), \quad (13)$$

repeated N times. To detect the preamble of this ED, the GW still uses the conventional DFT-based detector to calculate the signal of all M bins on all L antennas as in (3). Suppose the preamble $\boldsymbol{\rho}_u$ from the u th is received at time n :

$$\mathbf{y}_{n,\ell} = h_{u,\ell}\boldsymbol{\rho}_u + \boldsymbol{\omega}_{n,\ell}. \quad (14)$$

Since $\boldsymbol{\rho}_u$ is the sum of the two upchirps $\mathbf{s}_{\kappa_{u,1}}$ and $\mathbf{s}_{\kappa_{u,2}}$, the signal on M frequency bins is:

$$\tilde{\mathbf{V}}_{n,\ell}[k] = \begin{cases} \sqrt{\frac{M}{2}}h_{u,\ell} + \tilde{\mathbf{W}}_{n,\ell}[k], & k = \kappa_{u,1} \text{ or } \kappa_{u,2} \\ 0, & \text{otherwise.} \end{cases} \quad (15)$$

Let $\check{\mathbf{V}}_{n,k} = [\tilde{V}_{n,1}[k], \tilde{V}_{n,2}[k], \dots, \tilde{V}_{n,L}[k]]^\top \in \mathbb{C}^{L \times 1}$ be the signal vector collected on all L antennas in the k th bin at time n , the above equation can be rewritten in vector form as:

$$\check{\mathbf{V}}_{n,k} = \begin{cases} \sqrt{\frac{M}{2}}\mathbf{h}_u + \check{\mathbf{W}}_{n,k}, & k = \kappa_{u,1} \text{ or } \kappa_{u,2} \\ \check{\mathbf{W}}_{n,k}, & \text{otherwise,} \end{cases} \quad (16)$$

where $\check{\mathbf{W}}_{n,k} = [\tilde{W}_{n,1}[k], \tilde{W}_{n,2}[k], \dots, \tilde{W}_{n,L}[k]]^\top \in \mathbb{C}^{L \times 1}$ is the noise vector collected on all L antennas in the k th bin at time n . Thus, rather than performing a square-law combining and tracking the power of the corresponding bins of that ED as for the single ED case, the GW combines the signals over L antennas of the two bins $\check{\mathbf{V}}_{n,\kappa_{u,1}}$ and $\check{\mathbf{V}}_{n,\kappa_{u,2}}$ of the u th ED:

$$\begin{aligned}Z_{n,u} &= \frac{1}{L}\Re\left\{\check{\mathbf{V}}_{n,\kappa_{u,1}}^\top \check{\mathbf{V}}_{n,\kappa_{u,2}}\right\} \\ &= \frac{1}{L}\Re\left\{\left(\sqrt{\frac{M}{2}}\mathbf{h}_u + \check{\mathbf{W}}_{n,\kappa_{u,1}}\right)^\top \left(\sqrt{\frac{M}{2}}\mathbf{h}_u + \check{\mathbf{W}}_{n,\kappa_{u,2}}\right)\right\} \\ &= \frac{1}{L}\Re\left\{\sqrt{\frac{M}{2}}\mathbf{h}_u^\top (\check{\mathbf{W}}_{n,\kappa_{u,1}} + \check{\mathbf{W}}_{n,\kappa_{u,2}}) + \check{\mathbf{W}}_{n,\kappa_{u,1}}^\top \check{\mathbf{W}}_{n,\kappa_{u,2}}\right\} \\ &\quad + \frac{M}{2L}\|\mathbf{h}_u\|^2.\end{aligned}\quad (17)$$

For the remaining of this paper, $Z_{n,u} \in \mathbb{R}$ is referred to as the bin-combined preamble (BCP) signal of the u th ED. According to the law of large number [25], the term

$$\begin{aligned}\frac{1}{L}\Re\left\{\sqrt{\frac{M}{2}}\mathbf{h}_u^\top (\check{\mathbf{W}}_{n,\kappa_{u,1}} + \check{\mathbf{W}}_{n,\kappa_{u,2}}) + \check{\mathbf{W}}_{n,\kappa_{u,1}}^\top \check{\mathbf{W}}_{n,\kappa_{u,2}}\right\} \\ \xrightarrow[L \rightarrow \infty]{\text{a.s.}} 0,\end{aligned}\quad (18)$$

where $\xrightarrow[L \rightarrow \infty]{\text{a.s.}}$ denotes almost sure convergence when the number of antennas L tends to infinity [25]. This is because (18) consists of terms which are the multiplication between two statistically independent vectors [25]. On the other hand, also resulted from the law of large number

$$\frac{M}{2L}\|\mathbf{h}_u\|^2 \xrightarrow[L \rightarrow \infty]{\text{a.s.}} \frac{M}{2}. \quad (19)$$

As a result

$$Z_{n,u} \xrightarrow[L \rightarrow \infty]{\text{a.s.}} \frac{M}{2}. \quad (20)$$

Whereas, any other combinations of two bins other than between the $\kappa_{u,1}$ th and $\kappa_{u,2}$ th bins are just the multiplication between two independently distributed noise vectors, which will result in zero convergence

$$\frac{1}{L}\Re\left\{\check{\mathbf{V}}_{n,k_1}^\top \check{\mathbf{V}}_{n,k_2}\right\} = \frac{1}{L}\Re\left\{\check{\mathbf{W}}_{n,k_1}^\top \check{\mathbf{W}}_{n,k_2}\right\} \xrightarrow[L \rightarrow \infty]{\text{a.s.}} 0, \quad (21)$$

if $\{k_1, k_2\} \neq \{\kappa_{u,1}, \kappa_{u,2}\}$ [25]. Consequently, the *double-chirp* preamble $\boldsymbol{\rho}_u$ will not trigger any resembled PPs on the BCP signal $Z_{n,\tilde{u}}$ ($\tilde{u} \neq u$) of any other EDs at time n . Thus, this preamble design can reduce the chance that the preamble of the u th ED triggers the bins corresponding to the preambles of other EDs and causes preamble resemblance.

However, this preamble design still cannot completely get rid of the preamble resemblance effect that can make the

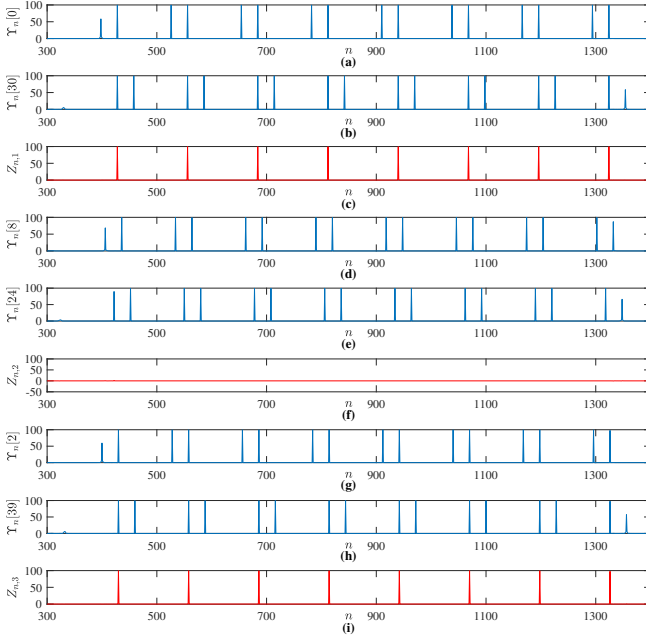


Fig. 5: Preamble signal of the first ED does not resemble the second ED, but resembles the third ED ($SF = 7$, $L = 64$, $\Delta_1 = \Delta_3 = 30$, $\Delta_2 = 16$).

GW make wrong decision on the preamble detection. In the following, Section III-B will study the preamble resemblances that are caused by *single-ED* sources, and how they can be eliminated with careful preamble assignment. Next, Section III-C will discuss the preamble resemblance that is jointly caused by *two different EDs*, which cannot be removed with preamble assignment, but can still be recognized by the GW.

B. Preamble resemblance from single-ED sources and the solution by preamble assignment

This subsection discusses the preamble resemblance of the proposed *double-chirp* preamble design that is caused by a *single ED*, and how to address it with preamble assignment.

1) *Inter-ED preamble resemblance*: Suppose the u th ED is assigned with chirps $s_{\kappa_{u,1}}$ and $s_{\kappa_{u,2}}$ as preamble, and the \tilde{u} th ED is assigned with $s_{1+\kappa_{u,1}}$ and $s_{1+\kappa_{u,2}}$. At time n , if

$$\mathbf{y}_{n,\ell} = h_{u,\ell} \boldsymbol{\rho}_u + \boldsymbol{\omega}_{n,\ell} = h_{m,\ell} \frac{1}{\sqrt{2}} (s_{\kappa_{u,1}} + s_{\kappa_{u,2}}) + \boldsymbol{\omega}_{n,\ell}, \quad (22)$$

then, similar to the single ED case in the previous section, at time $n+1$, when the detection window shifts by one sample

$$\begin{aligned} \mathbf{y}_{n+1,\ell} &= h_{u,\ell} \frac{1}{\sqrt{2}} (s_{1+\kappa_{u,1}} + s_{1+\kappa_{u,2}}) + \boldsymbol{\omega}_{n+1,\ell} \\ &= h_{u,\ell} \boldsymbol{\rho}_{\tilde{u}} + \boldsymbol{\omega}_{n+1,\ell}, \end{aligned} \quad (23)$$

which will trigger an unwanted PP in $Z_{n,\tilde{u}}$ for the \tilde{u} th ED at time $n+1$. Similarly, if another ED is assigned with $s_{\tau+\kappa_{u,1}}$ and $s_{\tau+\kappa_{u,2}}$ as preamble, it will also get unwanted PP at time $n+\tau$ if the preamble of the first ED is received at time n . This effect will be illustrated in the following example.

Example 1: This example illustrates how the proposed novel preamble design can enable preamble detection of an ED, and when preamble resemblance can occur.

Consider a LoRa network with 3 EDs and a GW with $L = 64$ antennas. Suppose the first ED is assigned with 2 chirps s_0 and s_{30} as preamble, the second ED is assigned with s_8 and s_{24} , and the third ED is assigned with s_2 and s_{32} . Assume that only the first ED is transmitting preamble with length $N = 8$. The power of the DFT output on the bins corresponding to the aforementioned chirps over time is illustrated in Fig. 5-(a). Since the first ED uses both s_0 and s_{30} as preamble, $2N = 16$ PPs in total appear on every bin $\Upsilon_n[k]$ ($k = 0, 1 \dots M-1$) when performing square-law combining, as shown in blue in Fig 5-(a), (b), (d), (e), (g), (h).

However, when combining two bins $\check{V}_{n,0}^H \check{V}_{n,30}$, which corresponds to the preamble of the first ED, only $N = 8$ PPs remain, as shown in red in Fig 5-(c). The reason is that s_0 and s_{30} are transmitted at the same time by the first ED. As a results, these two chirps trigger their own PPs on the corresponding bins (0th and 30th bins) at the same time, and hence, the combined signal from these two bins obtained with (21) also has PPs at the same position. On the other hand, the 8 PPs that s_0 triggers on the 30th bin, and the 8 PPs that s_{30} triggers on the 0th bin are not aligned. Thus, these unwanted peaks will not appear on the BCP signal $Z_{n,1}$ of the first ED.

Similarly, the PPs that the preamble of the first ED triggers on the 8th and 24th bins are not aligned either. Thus, the BCP signal of the second ED $Z_{n,2} = \check{V}_{n,8}^H \check{V}_{n,24}$ does not have any PPs resembled by the preamble of the first ED, as shown in Fig 5-(f). Thus, with this design, the preamble of the first ED can be detected by the GW, without resembling the preamble of the second ED.

However, the BCP signal $Z_{n,3} = \check{V}_{n,2}^H \check{V}_{n,32}$ of the third ED experiences $N = 8$ consecutive peaks similar to that of the first ED as shown in Fig. 5-(i). The reason is that after the PPs of the first ED is detected, when the detection window shifts in the time domain by two samples, s_0 becomes s_2 and s_{30} becomes s_{32} . As a consequence, the preamble of the first ED becomes identical to the preambles of the third ED, 2 samples after it was detected for the first ED, which leads to resembled preamble detection for the third ED. ■

Fortunately, this problem can be easily solved. Since the preamble constructed from the two chirps $s_{\kappa_{u,1}}$ and $s_{\kappa_{u,2}}$ will also resemble the preamble any ED that uses $s_{\kappa_{u,1}+\tau}$ and $s_{\kappa_{u,2}+\tau}$ as preamble, the undesirably PPs can be avoided by assigning preamble chirps to EDs such that the distance:

$$\Delta_u = \text{mod}(|\kappa_{u,1} - \kappa_{u,2}|, M/2), \quad (24)$$

is unique for each and every ED in the network. Since the LoRa chirp set is periodic with the period of M sample, this condition is generalized as

$$\Delta_u \neq \Delta_{\tilde{u}}, \forall u, \tilde{u}. \quad (25)$$

2) *Self preamble resemblance*: Unlike inter-ED preamble resemblance, where an ED's preamble can resemble that of other EDs, self preamble resemblance is caused by an ED to itself. This happens when the u th ED is assigned with two chirps s_{κ_u} and $s_{\kappa_u+M/2}$ as preamble. Suppose at time n , if

$$\mathbf{y}_{n,\ell} = h_{u,\ell} \boldsymbol{\rho}_u + \boldsymbol{\omega}_{n,\ell} = h_{u,\ell} \frac{1}{\sqrt{2}} (s_{\kappa_u} + s_{\kappa_u+M/2}) + \boldsymbol{\omega}_{n,\ell}, \quad (26)$$

then, similar to the explanation in previous subsection on the inter-ED case, at time $n + M/2$

$$\mathbf{y}_{n+M/2,\ell} = h_{u,\ell} \frac{1}{\sqrt{2}} (s_{\kappa_u+M/2} + s_{\kappa_u}) + \boldsymbol{\omega}_{n+M/2,\ell}, \quad (27)$$

which triggers a resembled PP of the same u th ED. Consequently, instead of having N consecutive PPs, separated by M samples, the BCP signal $Z_{n,u}$ of the u th ED will experience $2N$ PPs, separated by $M/2$ samples as shown in Fig. 6.

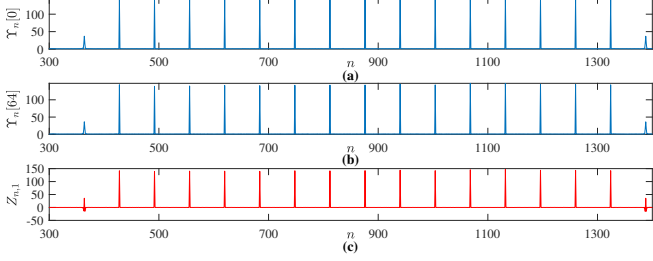


Fig. 6: Self preamble resemblance when an ED is assigned with s_0 and s_{64} as preamble. $2N = 16$ PPs appear instead of $N = 8$ PPs ($\Delta_m = 0$, SF = 7, $L = 64$).

As can be seen, this phenomenon only occurs when the double-chirp preamble has $|\kappa_{u,1} - \kappa_{u,2}| = M/2$. Thus, to avoid this problem, in addition to the condition in (25), the double-chirp preamble must also satisfy:

$$\Delta_u \neq 0, \forall u. \quad (28)$$

3) *ED limit with preamble assignment*: By the definition in (24), and with the constraint in (28), Δ_u must satisfy $0 < \Delta_u < M/2$. Since all Δ_u must be unique according to (25), the maximum number of EDs that can be supported without *single-ED* preamble resemblance is technically $(M/2 - 1)$.

C. Preamble resemblance from joint-ED source

In the previous subsection, the preamble resemblance caused by a single ED has been investigated. Fortunately, with the proposed preamble assignment method, the effect that the preamble of a single ED resembles the preambles of other EDs (and/or itself) can be avoided. However, this only prevents an ED from resembling, *single-handedly*, the preamble of other EDs. In this subsection, we examine another case of preamble resemblance that involves two different EDs *jointly* resembling the preamble of a third ED.

Without the loss of generality, suppose the first ED transmits the preamble $\rho_1 = [(s_{\kappa_{1,1}} + s_{\kappa_{1,2}})]/\sqrt{2}$ at time n and the second ED transmits the $\rho_2 = [(s_{\kappa_{2,1}} + s_{\kappa_{2,2}})]/\sqrt{2}$ at time $n + \tau$ (where $\tau < M$), we have:

$$\mathbf{y}_{n+\tau,\ell} = \frac{h_{1,\ell}(s_{\kappa_{1,1}+\tau} + s_{\kappa_{1,2}+\tau}) + h_{2,\ell}(s_{\kappa_{2,1}} + s_{\kappa_{2,2}})}{\sqrt{2}} + \boldsymbol{\omega}_{n+\tau,\ell}, \quad (29)$$

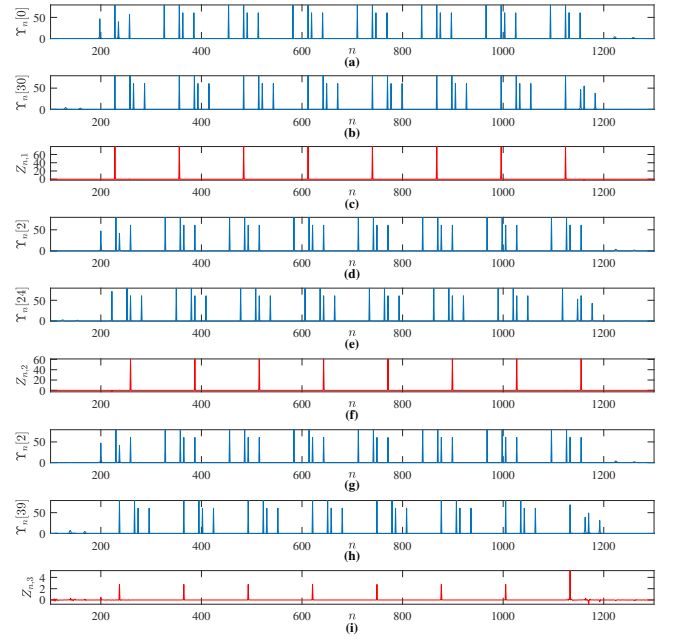


Fig. 7: The first and the second EDs' preamble do not resemble the preamble of each other, but jointly resemble the preamble of the third ED (SF = 7, $L = 64$).

As a result, at time $n + \tau$:

$$\tilde{V}_{n+\tau,\ell}[k] = \begin{cases} \sqrt{\frac{M}{2}} h_{1,\ell} + \tilde{W}_{n+\tau,\ell}[k], & k \in \{\kappa_{1,1} + \tau, \kappa_{1,2} + \tau\} \\ \sqrt{\frac{M}{2}} h_{2,\ell} + \tilde{W}_{n+\tau,\ell}[k], & k \in \{\kappa_{1,1}, \kappa_{1,2}\} \\ \tilde{W}_{n+\tau,\ell}[k], & \text{otherwise.} \end{cases} \quad (30)$$

Consequently, the preamble of these two EDs can resemble the preamble of a third ED that is assigned with $s_{\kappa_{3,1}}$ and $s_{\kappa_{3,2}}$ as preamble, if $\kappa_{3,1}$ and $\kappa_{3,2}$ take on the values in $\{\kappa_{1,1} + \tau, \kappa_{1,2} + \tau, \kappa_{2,1}, \kappa_{2,2}\}$. In this case:

$$Z_{n+\tau,3} = \frac{1}{L} \Re \left\{ \check{V}_{n+\tau,\kappa_{3,1}}^H \check{V}_{n+\tau,\kappa_{3,2}} \right\} = \frac{1}{L} \Re \left\{ \left(\sqrt{\frac{M}{2}} \mathbf{h}_1 + \check{W}_{n+\tau,\kappa_{3,1}} \right)^H \left(\sqrt{\frac{M}{2}} \mathbf{h}_2 + \check{W}_{n+\tau,\kappa_{3,2}} \right) \right\} \xrightarrow[L \rightarrow \infty]{\text{a.s.}} 0, \quad (31)$$

since \mathbf{h}_1 and \mathbf{h}_2 are statistically independent, according to the law of large number [25].

Although $Z_{n+\tau,3}$ converges to zero when L tends to infinity, with a limited number of antennas, $Z_{n+\tau,3}$ still experiences preamble resemblance. This is due to the correlation between \mathbf{h}_1 and \mathbf{h}_2 , which is independent of n , and results in the consecutive peaks, despite being of low amplitudes compared to true PPs. This effect will be shown in the next example.

Example 2: This example shows how two different EDs can resemble the preamble of a third ED.

Consider a LoRa network with 3 EDs and a GW with $L = 64$ antennas. Suppose the first ED is assigned with 2 chirps s_0 and s_{30} as preamble, and the second ED is assigned with s_2 and s_{24} , and the third ED is assigned with s_2 and s_{39} . Assume that the first and the second are transmitting their preambles,

while the third ED is idle. The time of arrival (ToA) of the first ED is $n = 0$ and the ToA of the second is $n = 31$.

The BCP signals of the first and the second EDs $Z_{n,1}$ and $Z_{n,2}$ are shown in Fig. 7-(c) and (f), respectively. As can be seen, with the double-chirp design with non-zero $\Delta_1 \neq \Delta_2$, the preamble of each ED does not resemble the preamble of the other. Thus, the transmitted preambles of the first and second EDs can be detected without preamble resemblance.

However, while observing the BCP signal $Z_{n,3}$ of the third ED, the GW will also see consecutive PPs even though the third ED is idle as shown in Fig. 7-(i). The reason is that at time $n = 9$, the chirp s_{30} (belongs to the first ED) will become s_{39} (shifted 9 samples to the right). Whereas, the chirp s_{24} of the second ED will become s_2 (shifted 9 samples to the right, then 31 samples to the left since the ToA of the second ED is 31 samples later than the first ED). Consequently, $Z_{n,3}$ will experience N PPs as a result of the correlation between chirp s_{30} of the first ED and chirp s_{24} of the second ED.

From Fig. 7-(i), it can be seen that the amplitude of these resembled PPs are of small values in comparison with the true PPs of the first and the second EDs, since the channels of the first and the second EDs are independent. However, they can still potentially be mistaken as a true preamble. ■

Unlike single-ED preamble resemblance that can be avoided with preamble assignment, joint-ED preamble resemblance cannot be. Its occurrence depends on the randomness of the difference between the ToAs of two EDs. Consequently, the resembled preamble caused by joint-ED accounts for the major number of errors in preamble detection in multiuser massive MIMO LoRa networks. Fortunately, thanks to the statistical independence among channels of different EDs to the GW, the resembled PPs caused by joint-ED preamble resemblance are mostly of low amplitudes, and are equally likely to be either positive or negative. This results in the statistical difference between a resembled preamble and a true one, which has the PPs most certainly of positive amplitude with the mean of $M/2$ as shown in (17). Based on this statistical difference, in the next section, we will derive a maximum-likelihood (ML) based receiver, which determines the presence of an ED's preamble by measuring the likelihood of it being a true preamble, or a resembled one, or noise/interference.

IV. ML-BASED NON-COHERENT DETECTION FOR DOUBLE-CHIRP PREAMBLE DESIGN

Since a preamble consists of N consecutive identical symbols, in the presence of a new packet from the u th ED, the GW would expect to observe N consecutive PPs, equally spaced by M samples, when observing $Z_{n,u}$, as shown in Fig. 6. Let:

$$Z_{n,u} = [Z_{n-M(N-1),u}, Z_{n-M(N-2),u}, \dots, Z_{n,u}]^T \in \mathbb{C}^{N \times 1}, \quad (32)$$

which is obtained by taking N samples, separated by M samples, from the BCP signal $Z_{n,u}$ of the u th ED. Conventionally, the preamble can be detected with majority vote method [15], which means that when at least N_{thr} out of N elements of the BCP signal $Z_{n,u}$ have the magnitudes greater than a predetermined threshold, the GW will determine that the preamble of the u th is present.

However, this approach does not take into account the statistical dependency of the consecutive PPs in the case of block fading channel, when the channel are assumed to be constant over a coherence time. It also overlooks the consecutive structure of a preamble, and the possibility of other error events caused by interference. In the remaining of this section, we study the likelihood of a preamble, which takes into account the preamble structure and the statistical dependency between PPs, and the likelihoods of other error events that can corrupt the preamble detection in multiuser LoRa networks to derive a ML-based non-coherent preamble detector. In specific the likelihood function of $Z_{n,u}$ will be derived for the following cases preamble, resembled preamble caused by joint-EDs, and noise plus interference.

A. Likelihood of noise

To determine when a preamble is present, it is also important to know when there is not. Therefore, first the likelihood that $Z_{n,u}$ is noise must be evaluated. It can be seen that, when no ED is transmitting, the $L \times 1$ signal vector $\check{V}_{n,k}$ received on L antennas on the k th bin at time n is given as:

$$\check{V}_{n,k} = \check{W}_{n,k}, \quad \forall k. \quad (33)$$

As a result, the BCP signal of the u th at time n becomes

$$\begin{aligned} Z_{n,u} &= \frac{1}{L} \Re \left\{ \check{V}_{n,\kappa_{u,1}}^H \check{V}_{n,\kappa_{u,2}} \right\} = \frac{1}{L} \Re \left\{ \check{W}_{n,\kappa_{u,1}}^H \check{W}_{n,\kappa_{u,2}} \right\} \\ &= \frac{1}{L} \sum_{\ell=1}^L \Re \left\{ \left(\check{W}_{n,\ell}[\kappa_{u,1}] \right)^* \check{W}_{n,\ell}[\kappa_{u,2}] \right\}. \end{aligned} \quad (34)$$

To derive the likelihood function of $Z_{n,u}$ being noise, its statistic must be examined. However, the exact distribution of $Z_{n,u}$, which is the real part of the product of two complex-normal distributed random vectors, is rather sophisticated. Thus, instead of finding the exact distribution for $Z_{n,u}$ in this case, an approximated Gaussian distribution is derived as in Lemma 1 following the central limit theorem [26].

Lemma 1. *When the BCP signal of the u th ED at time n contains only noise, the distribution of $Z_{n,u}$ can be approximated as $Z_{n,u} \sim \mathcal{N}(0, \sigma_n^2)$, where $\sigma_n = \sigma^4/2L$.*

Proof: Please refer to Appendix A. □

From Lemma 1, it can be easily seen that the likelihood function that all N elements of $Z_{n,u}$ is:

$$\mathcal{L}^{(n)}(Z_{n,u}) = f(Z_{n,u} | \text{noise}) = \frac{\exp \left\{ -\frac{\|Z_{n,u}\|^2}{2\sigma_n^2} \right\}}{\left(\sqrt{2\pi\sigma_n^2} \right)^N}, \quad (35)$$

where $f(Z_{n,u} | \text{noise})$ is the probability distribution function (pdf) that all N elements of $Z_{n,u}$ contain only noise.

B. Likelihood of true preamble from a single ED

Similar to the case of noise, when $Z_{n,u}$ is a PP, it is also the sum of L i.i.d random variables. Likewise, in this case, the distribution of $Z_{n,u}$ can be approximated in Lemma 2 following the central limit theorem [26].

Lemma 2. When the BCP signal of the u th ED at time n is a PP, the distribution of $Z_{n,u}$ can be approximated as a Gaussian random variable $Z_{n,u} \sim \mathcal{N}\left(\frac{M}{2}, \sigma_{\text{PP}}^2\right)$, where $\sigma_{\text{PP}}^2 = M^2/4L + M\sigma^2/2L + \sigma^4/2L$.

Proof: Please refer to Appendix B. \square

From Lemma 1 and 2, one can easily derive a threshold to determine whether $Z_{n,u}$ is noise or a PP. Then, conventionally, by counting if the number of PPs in $Z_{n,u}$ exceed a predetermined number, the GW can declare if a preamble is present. However, this decision rule overlooks two important properties of the LoRa preamble, which can be utilized to enhance the preamble detection performance:

- The consecutive structure of LoRa preamble: since the LoRa preamble arrives as N consecutive identical symbols, if p elements of $Z_{n,u}$ are PPs ($p \leq N$), their positions in the vector $Z_{n,u}$ are not random, but must be either the first p or the last p elements of $Z_{n,u}$. The last p elements of $Z_{n,u}$ being PPs means that the first p symbols of the preamble have arrived. Whereas, the first p elements of $Z_{n,u}$ being PPs means that the preamble has been over and its last p symbols are leaving $Z_{n,u}$.
- The statistical dependency among the PPs: from (17), it can be seen that the third term $M\|\mathbf{h}_u\|^2/2L$ of $Z_{n,u}$ does not depend on n . It appears in every PP element of $Z_{n,u}$ and results in the statistical dependency of these PPs. By establishing the joint distribution of the PPs in $Z_{n,u}$, a more precise likelihood function for the preamble can be achieved rather than examining the PPs individually as in conventional LoRa preamble detection.

Based on Lemma 1 and 2, the distribution of $Z_{n,u}$ given that p out of its N elements are PPs is given in Corollary 1.

Corollary 1. The distribution of $Z_{n,u}$ given that the p first elements are PPs can be approximated as a multivariate Gaussian distribution with pdf:

$$f(Z_{n,u}|\text{first } p \text{ PPs}) = \frac{\exp\left(-\frac{(Z_{n,u} - \mu_p)^H \Sigma_p^{-1} (Z_{n,u} - \mu_p)}{2}\right)}{(2\pi)^{N/2} \sqrt{\det(\Sigma_p)}}, \quad (36)$$

where μ_p is the mean vector with the element $\mu_{p,i} = \frac{M}{2}$ for $i \leq p$ or $\mu_{p,i} = 0$, otherwise, and the elements of the covariance matrix Σ_p are

$$\Sigma_{p,i,j} = \begin{cases} \sigma_{\text{PP}}^2, & i = j \leq p \\ \sigma_n^2, & i = j > p \\ \frac{M^2}{4L}, & i < j \leq p \\ \frac{M^2}{4L}, & j < i \leq p \\ 0, & \text{otherwise.} \end{cases} \quad (37)$$

Likewise, the pdf of $Z_{n,u}$ when the last p elements are PPs $f(Z_{n,u}|\text{last } p \text{ PPs})$ is similar to (36), but with the mean vector μ_p replaced by $\tilde{\mu}_p$, where $\tilde{\mu}_{p,i} = \mu_{p,N-i+1}$, and the covariance matrix Σ_p replaced by $\tilde{\Sigma}_p$, whose element $\tilde{\Sigma}_{p,i,j} = \Sigma_{p,N-i+1,N-j+1}$.

Proof: Please refer to Appendix C. \square

From Corollary 1, the likelihood function that a part of the preamble of the u th ED is present in $Z_{n,u}$ is given as:

$$\begin{aligned} \mathcal{L}^{(\text{p})}(Z_{n,u}) = & \sum_{p=N_{\text{thr}}}^N f(Z_{n,u}|\text{first } p \text{ PPs}) \\ & + \sum_{p=N_{\text{thr}}}^{N-1} f(Z_{n,u}|\text{last } p \text{ PPs}). \end{aligned} \quad (38)$$

Note that the two sums in the above equation only run from $N = N_{\text{thr}}$, which is the minimum number of PPs required in $Z_{n,u}$ to declare a preamble. This is to lower the chance that noise and interference can be mistaken to a true preamble when the required number of PPs is too low. A higher value of N_{thr} means a stricter condition to declare a preamble, which lower the probability of mistaking noise and interference to true preambles, but can also increase the probability of missing the presence under the influence of fading, noise and interference. By contrast, a lower value of N_{thr} results in the opposite. In the simulation results, the changes in preamble detection performance when varying N_{thr} will be observed.

In addition, the second sum only runs from N_{thr} to $N - 1$, since with $p = N$, $f(Z_{n,u}|\text{first } p \text{ PPs})$ and $f(Z_{n,u}|\text{last } p \text{ PPs})$ are the same, which is when all N elements of $Z_{n,u}$ are PPs. Thus, the value of $f(Z_{n,u}|\text{last } i \text{ PPs})$ for $p = N$ is discarded to avoid duplicate.

C. Likelihood of resembled preamble

Similar to the case of true preambles, resemble preambles also have the consecutive-identical-symbol structure and the dependency between resembled PPs (RPPs). Thus, the distribution of resembled PPs must be derived similar to a true preamble. First, the distribution of $Z_{n,u}$ given that it is a RPP can be found as in Lemma 3 below.

Lemma 3. When the BCP signal of the u th ED at time n is a RPP, the distribution of $Z_{n,u}$ can be approximated as $Z_{n,u} \sim \mathcal{N}(0, \sigma_{\text{R}}^2)$, where $\sigma_{\text{R}}^2 = M^2/8L + M\sigma^2/2L + \sigma^4/2L$.

Proof: The proof of this lemma is straightforward and can be performed similar to that of Lemma 2. \blacksquare

Similar to the case of true preamble, considering the consecutive-identical-symbol structure of preamble resemblance, the distribution of $Z_{n,u}$ given that p out of N of its elements are RPP can be derived as in the following Corollary.

Corollary 2. The distribution of $Z_{n,u}$ given that the p first elements are RPPs can be approximated as a multivariate Gaussian distribution with pdf:

$$f(Z_{n,u}|\text{first } p \text{ RPPs}) = \frac{\exp\left(-\frac{Z_{n,u}^H \Psi_p^{-1} Z_{n,u}}{2}\right)}{(2\pi)^{N/2} \sqrt{\det(\Psi_p)}}, \quad (39)$$

where the elements of the covariance matrix Ψ_p are

$$\Psi_{p,i,j} = \begin{cases} \sigma_{\text{R}}^2, & i = j \leq p \\ \sigma_n^2, & i = j > p \\ \frac{M^2}{8L}, & i < j \leq p \\ \frac{M^2}{8L}, & j < i \leq p \\ 0, & \text{otherwise.} \end{cases} \quad (40)$$

Likewise, the pdf of $\mathbf{Z}_{n,u}$ when the last p elements are RPPs $f(\mathbf{Z}_{n,u}|\text{last } p \text{ RPPs})$ is similar to (39), but with the covariance matrix Ψ_p replaced by $\tilde{\Psi}_p$, whose element $\tilde{\Psi}_{p,i,j} = \Psi_{p,N-i+1,N-j+1}$.

Proof: The proof of this corollary is straightforward and can be performed similar to that of Corollary 1. \blacksquare

From Lemma 3, the likelihood that $\mathbf{Z}_{n,u}$ contains a part of a resembled preamble can be calculated as:

$$\begin{aligned} \mathcal{L}^{(r)}(\mathbf{Z}_{n,u}) &= \sum_{p=1}^N f(\mathbf{Z}_{n,u}|\text{first } p \text{ RPPs}) \\ &+ \sum_{p=1}^{N-1} f(\mathbf{Z}_{n,u}|\text{last } p \text{ RPPs}). \end{aligned} \quad (41)$$

Similar to the case of true preamble, the second sum in (41) only runs from $p = 1$ to $N - 1$ to avoid duplicate.

D. Likelihood of other interference

In order for the \tilde{u} th ED to interfere with the BCP signal $\mathbf{Z}_{n,u}$ of the u th ED, its signal $\bar{\mathbf{x}}_{n,\tilde{u}}$ must simultaneously occupies the $\kappa_{u,1}$ th and $\kappa_{u,2}$ th bin. According to the analysis in Section III-B, this cannot be caused by the preamble of the \tilde{u} th ED, thanks to the preamble design and assignment. However, this can happen when $\bar{\mathbf{x}}_{n,\tilde{u}}$ contains the fragments of two different chirps, when the detection window is moving from one symbol to the next one, as analyzed in Section III-B. According to Fig 2, the amplitudes of the bins when $\bar{\mathbf{x}}_{n,\tilde{u}}$ contains the fragments of two different chirps are of small values. Thus, this type of interference can be treated as part of the noise.

The interference can also be jointly caused by multiple EDs, the same way resembled preambles are created. However, thanks to the asymptotic orthogonality among different ED's channels, this type of interference converges to zero when the number of antennas tends to infinity [25]. Since this type of interference is also of zero mean and small amplitudes, it can also be treated as noise.

Thus, in this paper, we do not derive the distribution for interference. The reason is that the interaction between the signals of multiple EDs (causes joint-interference from multiple EDs), and different fragments of chirps (causes interference from a single ED) are extremely complicated, and is mostly intractable. In addition, as discussed above, the characteristic of interference can be reasonably treated as noise. This is also a common assumption in existing works in preamble detection [15], [20], [22].

E. ML-based non-coherent double-chirp preamble detection

From the above likelihood functions, the preamble detection rule for the u th ED can be established as follows:

$$\mathcal{L}^{(p)}(\mathbf{Z}_{n,u}) \stackrel{\text{preamble}}{\gtrless} \mathcal{L}^{(n)}(\mathbf{Z}_{n,u}) + \mathcal{L}^{(r)}(\mathbf{Z}_{n,u}). \quad (42)$$

Once this condition is satisfied, the GW will determine that the preamble of the u th ED is present. The proposed ML-based preamble detection method for multiuser massive MIMO LoRaWAN is summarized in the following Algorithm 1.

Algorithm 1 ML-based double-chirp preamble detection

Require: Number of EDs, SF, preamble assignment.

```

1: AllDetected = 0, counter[ $u$ ] = 0,  $\forall u$ , last[ $u$ ] = 0
2: while AllDetected = 0 do
3:   Performing dechirped-FFT to obtain  $\check{\mathbf{V}}_{n,\ell}, \forall \ell$ ;
4:   for  $u = 1$  to  $N_u$  do
5:     Calculating  $\mathbf{Z}_{n,u}$ , and likelihood functions (35), (38), (41);
6:     if  $\mathcal{L}^{(p)}(\mathbf{Z}_{n,u}) > \mathcal{L}^{(n)}(\mathbf{Z}_{n,u}) + \mathcal{L}^{(r)}(\mathbf{Z}_{n,u})$  then
7:       Preamble detected for the  $u$ th ED;
8:     end if
9:   end for
10:  if All preambles are detected then
11:    AllDetected = 1;
12:  end if
13:   $n = n + 1$ ;
14: end while
15: return All detected preamble.

```

V. COMPLEXITY REDUCTION

Since the detection for double-chirp preamble design requires computation *every sample* (rather than every LoRa symbol as the methods in [16]–[19]), the complexity can be an issue with practical implementation. Thus, in this section, we provide the complexity analysis for the detection of the proposed double-chirp preamble, and how to reduce that for practical implementation.

With the Fast Fourier Transform (FFT), the complexity of performing the dechirped-FFT on all L antennas requires $\mathcal{O}(LM\log_2 M)$. Then, to obtain the preamble BCP signal in (17) of all N_u EDs, the complexity is $\mathcal{O}(N_u L)$. The calculation of the likelihood functions (35), (38), (41) for all N_u EDs requires $\mathcal{O}(N_u N^3)$. As a result, the overall computational complexity to simultaneously detect the preambles of N_u EDs is $\mathcal{O}(LM\log_2 M + N_u L + N_u N^3)$ every sample. Since M is significantly larger than N_u , L and N , it can be seen that the most computationally demanding task is the FFT. Thus, we propose the following technique to relax the GW from having to compute the FFT for every sample.

Suppose that the bin signal vectors $\mathbf{V}_{n,\ell}$ on all M bins in the FFT domain is calculated in (3) for time n . From this equation, the bin signals corresponding to time $n + 1$ is:

$$\mathbf{V}_{n+1,\ell} = \text{DFT} \{ \mathbf{y}_{n+1,\ell} \otimes \mathbf{s}_0^* \} \in \mathbb{C}^{M \times 1}. \quad (43)$$

Since $\mathbf{y}_{n+1,\ell} = (\mathbf{y}_{n,\ell} \ll 1) + [0, 0 \dots 0, \delta_{n+1}]^\top$, where $\delta_{n+1} = y_{n+M,\ell} - y_{n+M-1,\ell}$, we have:

$$\begin{aligned} \mathbf{y}_{n+1,\ell} \otimes \mathbf{s}_0^* &= (\mathbf{y}_{n,\ell} \ll 1) \otimes \mathbf{s}_0^* + [0, \dots 0, \delta_{n+1}]^\top \otimes \mathbf{s}_0^* \\ &= ((\mathbf{y}_{n,\ell} \otimes (\mathbf{s}_0^* \gg 1)) \ll 1) + \mathbf{d}, \end{aligned} \quad (44)$$

with $\mathbf{d} = \mathbf{s}_{0,m}^* [0, \dots 0, \delta_{n+1}]^\top$. Plugging (44) into (43) yields:

$$\begin{aligned} \mathbf{V}_{n+1,\ell} &= \text{DFT} \{ ((\mathbf{y}_{n,\ell} \otimes (\mathbf{s}_0^* \gg 1)) \ll 1) + \mathbf{d} \} \\ &= \text{DFT} \{ (\mathbf{y}_{n,\ell} \otimes \mathbf{s}_1^*) \ll 1 \} + \text{DFT} \{ \mathbf{d} \}. \end{aligned} \quad (45)$$

The second term of (45) is the DFT of a vector with only one non-zero element, which can be easily calculated in $\mathcal{O}(M)$ without using the FFT. Whereas, following the shifting properties of the DFT, the first term of (45) can be found as:

$$\text{DFT} \{ (\mathbf{y}_{n,\ell} \otimes \mathbf{s}_1^*) \ll 1 \} = \boldsymbol{\alpha} \otimes \text{DFT} \{ \mathbf{y}_{n,\ell} \otimes \mathbf{s}_1^* \} \quad (46)$$

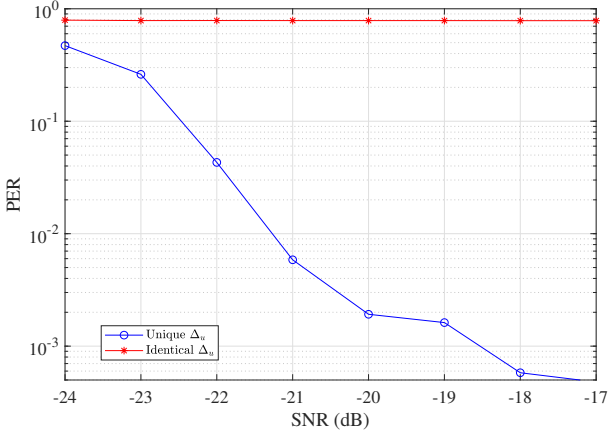


Fig. 8: PER with different preamble assignment ($L = 32$, $N = 8$, $N_{\text{thr}} = 4$)

where $\boldsymbol{\alpha} = [\alpha[0], \alpha[1] \dots \alpha[M-1]]$ and $\alpha[k] = \exp\{j2\pi k/M\}$. Next, since

$$\begin{aligned} s_{1,m} = s_{0,m+1} &= \exp \left\{ j2\pi \left(\frac{m^2}{2M} - \frac{m}{2} \right) \right\} \\ &= \exp \left\{ j2\pi \left(\frac{1}{2} - \frac{1}{2M} \right) \right\} \exp \left\{ j2\pi \frac{m-1}{M} \right\} s_{0,m}, \end{aligned} \quad (47)$$

we have

$$\begin{aligned} \text{DFT} \{ \mathbf{y}_{n,\ell} \otimes \mathbf{s}_1^* \} &= \\ &= \exp \left\{ j2\pi \left(\frac{1}{2} - \frac{1}{2M} \right) \right\} \text{DFT} \{ \mathbf{y}_{n,\ell} \otimes \mathbf{s}_0^* \} \gg 1 \quad (48) \\ &= \exp \left\{ j2\pi \left(\frac{1}{2} - \frac{1}{2M} \right) \right\} \mathbf{V}_{n,\ell} \gg 1. \end{aligned}$$

Plugging (46), (48) into (45), we have:

$$\mathbf{V}_{n+1,\ell} = \tilde{\boldsymbol{\alpha}} \otimes (\mathbf{V}_{n,\ell} \gg 1) + \text{DFT} \{ \mathbf{d} \}, \quad (49)$$

where $\tilde{\boldsymbol{\alpha}} = \exp \left\{ j2\pi \left(\frac{1}{2} - \frac{1}{2M} \right) \right\} \boldsymbol{\alpha}$. This equation suggests that, when detecting preamble in every sample, only the first sample needs FFT at time n . The bin signals in the frequency domain of succeeding samples $\mathbf{V}_{n+1,\ell}$ at time $n+1$ can be calculated sequentially as (49) with the complexity of $\mathcal{O}(M)$, rather than $\mathcal{O}(M \log_2 M)$ when using FFT. Consequently, the overall complexity to process one sample with the proposed preamble design is $\mathcal{O}(LM + N_u L + N_u N^3)$.

VI. SIMULATION RESULTS

In this section, simulation results are provided to show the merits of the proposed scheme. We consider a single GW with varying number of antennas, receiving packets from multiple EDs. The simulation results are averaged over 10^4 iterations. In every iteration, the packets from all EDs, the ToA, the channel vectors are randomly generated. Each ED is assumed to send one packet with SF = 7 and random ToA, with the payload lengths uniformly distributed from 20 to 30 symbols. The packets from different EDs are generated with the ToA differences following exponential distribution with the mean of one packet per one LoRa symbol duration.

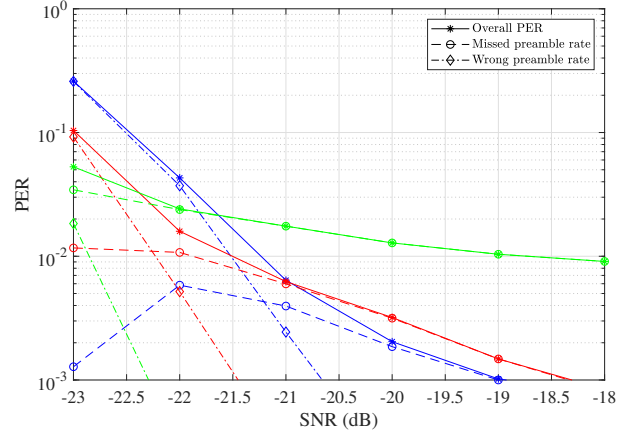
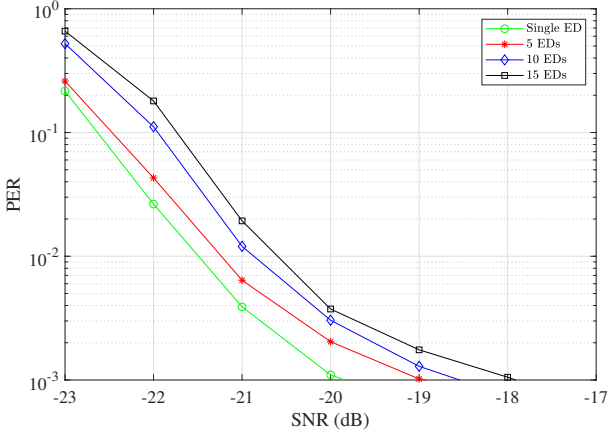
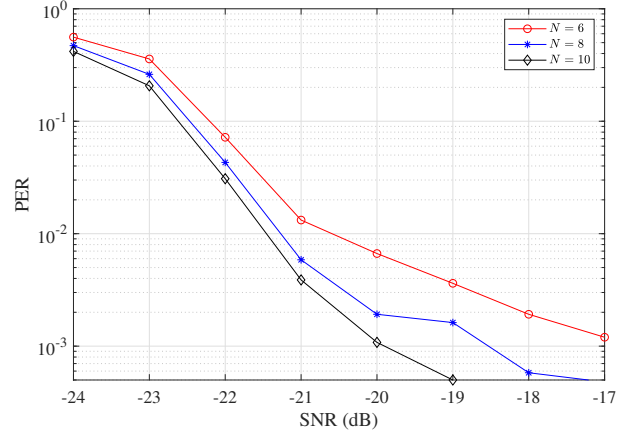
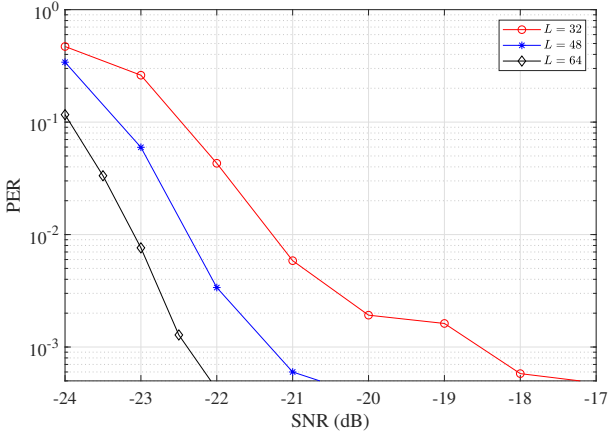


Fig. 9: PER with different threshold numbers of PPs ($N = 8$, $L = 32$, 5 EDs). Blue, red and green lines are for $N_{\text{thr}} = 4$, 5 and 8, respectively.

Fig. 8 shows the effect of preamble assignment to the preamble error rate (PER) of the proposed design. When all EDs have the same Δ_u , resembled preamble caused by single-ED sources will certainly occur, which results in a very poor PER as can be seen in the red figure. Fortunately, this can be avoided with preamble assignment by setting unique values of Δ_u for every EDs, which can be seen in blue. Given the importance of preamble assignment, in the remaining figures, the simulation results are obtained when the preambles are assigned with unique values of Δ_u .

Fig. 9 shows the effect of the threshold number of PPs N_{thr} on the preamble detection performance of the proposed design. Although the overall PER are somewhat equivalent when $N_{\text{thr}} = 4$ or 6 PPs, the differences in missed preamble rate (the GW fails to detect the presence of a preamble) and wrong preamble rate (the GW mistakes noise and interference to true preamble) are significant. With the larger value of N_{thr} , the missed preamble rate is significantly higher. As discussed earlier, the reason is that higher values of PPs required to declare a preamble means a stricter condition that can result in more missed preamble. This, however, will be able to obtain a lower chance of mistaking noise and interference to true preamble. This becomes more evident when $N_{\text{thr}} = 8$, when the wrong preamble rate is significantly lower than that of the two previous cases, but the missed preamble rate is much higher than when $N_{\text{thr}} = 4$ or 6. Given that at higher SNR range, the missed preamble rate becomes the dominant source of errors, $N_{\text{thr}} = 4$ appears to be a good choice for the balance between missed preamble rate and wrong preamble rate, which results in a better overall PER. In the remaining figures, the simulation results shall be obtained with $N_{\text{thr}} = 4$.

Fig. 10 shows the PER with different numbers of EDs. An error in preamble detection is defined as when the GW fails to recognize the presence of a preamble, or mistakes noise, interference or resembled preambles as true ones. Obviously, the PER increases when there are more EDs concurrently transmitting packets, which results in more interference and a higher chance of resembled preamble occurring. According to the figure, at the PER of 10^{-3} , the proposed preamble design

Fig. 10: PER with different numbers of EDs ($L = 32, N = 8$)Fig. 12: PER with different preamble lengths ($L = 32, 5$ EDs)Fig. 11: PER with different numbers of antennas ($N = 8, 5$ EDs)

required 2 dB more power to serve 15 EDs, as compared to the single-ED case. This appears to be a good trade-off to increase the connectivity and capacity in LoRaWAN.

Fig. 11 shows the PER of the proposed preamble design with different numbers of antennas. With a higher number of antennas, the noise and interference can be further suppressed, which explained the declining PER when the number of antennas increases. It can be seen that by doubling the number of antennas from 32 to 64, the proposed design can save around 4 dB transmit power to achieve the PER of 10^{-3} .

Fig. 12 compares the PER performance with different preamble lengths. According to the standard [8], the length of LoRa preamble is $N = 6$ to 8 LoRa symbols. The difference of two symbols in preamble length results in a gap of 1.5 dB to obtain the PER of 10^{-3} . Extending the length of the preamble to 10 symbols leads to an extra gain of nearly 2 dB gain in power to achieve the same PER. Although a longer preamble means more airtime to transmit a packet of the same payload, the power gain can still be a good trade-off, especially in IoT applications that requires long battery life.

VII. CONCLUSION

This paper proposed a novel *double-chirp* preamble design for multiuser massive MIMO LoRa networks, which allows LoRa GWs to detect asynchronous packets from multiple EDs simultaneously. First, we show that the challenge that prevents conventional *single-chirp* preamble design from multiuser detection is the so-called *preamble resemblance* effect. Then, we proposed the novel *double-chirp* preamble design to mitigate *preamble resemblance*. Next, we proposed a ML-based preamble detection algorithm to increase the reliability and reduce confusion between true preambles and noise plus interference. Finally, since our proposed method requires computation for every sample, we proposed a complexity reduction technique to efficiently calculate the DFT recursively rather than performing FFT every sampling period. Simulation results show that the proposed preamble design enables the GW to simultaneously detect preambles of multiple EDs with a reasonable power cost of roughly 2 dB to increase the number of EDs from one to 15. It has also been shown that the use of multiple antenna GW is necessary to mitigate the influence of noise and interference, which is evident from a gain of 4 dB achieved by doubling the number of antennas from 32 to 64.

APPENDIX A PROOF OF LEMMA 1

According to (34), $Z_{n,u}$ is the sum of L identically independently distributed (i.i.d) random variables. Thus, as a result of the central limit theorem [26], $Z_{n,u}$ can be approximated as a Gaussian random variable with the mean and variance being the sum of the means and variances of the addend random variables. Since $\tilde{W}_{n,\ell}[k] \sim \mathcal{CN}(0, \sigma^2)$, $\forall k$, it can be easily seen that: $\mathbb{E} \left\{ \Re \left\{ \left(\tilde{W}_{n,\ell}[\kappa_{u,1}] \right)^* \tilde{W}_{n,\ell}[\kappa_{u,2}] \right\} \right\} = 0$, and $\text{Var} \left\{ \Re \left\{ \left(\tilde{W}_{n,\ell}[\kappa_{u,1}] \right)^* \tilde{W}_{n,\ell}[\kappa_{u,2}] \right\} \right\} = \frac{\sigma^4}{2}$. Consequently, by adding up over all L antennas, the approximated distribution of $Z_{n,u}$ in Lemma 1 can be obtained. ■

APPENDIX B PROOF OF LEMMA 2

The proof of this lemma can be done similar to the proof of Lemma 1, where the mean and variance of each individual

addend random variable on the ℓ th antenna is derived. From (17), it can be seen that when $Z_{n,u}$ is a PP:

$$Z_{n,u} = \frac{1}{L} \sum_{\ell=1}^L \Re \left\{ \sqrt{\frac{M}{2}} h_{u,\ell}^* \left(\tilde{W}_{n,\kappa_{u,1}} + \tilde{W}_{n,\kappa_{u,2}} \right) \right\} + \frac{1}{L} \sum_{\ell=1}^L \Re \left\{ \left(\tilde{W}_{n,\ell}[\kappa_{u,1}] \right)^* \tilde{W}_{n,\ell}[\kappa_{u,2}] \right\} + \frac{M}{2L} \|\mathbf{h}_u\|^2. \quad (50)$$

The mean and variance of the three terms in (50) must be computed to derive the approximation of $Z_{n,u}$ as a PP.

- First, since $h_{u,\ell}$, $\tilde{W}_{n,\kappa_{u,1}}$ and $\tilde{W}_{n,\kappa_{u,2}}$ are independent, it can be easily seen that: $\mathbb{E} \left\{ \Re \left\{ h_{u,\ell}^* \left(\tilde{W}_{n,\kappa_{u,1}} + \tilde{W}_{n,\kappa_{u,2}} \right) \right\} \right\} = 0$, and $\text{Var} \left\{ \Re \left\{ h_{u,\ell}^* \left(\tilde{W}_{n,\kappa_{u,1}} + \tilde{W}_{n,\kappa_{u,2}} \right) \right\} \right\} = \sigma^2$.
- The mean and variance of the second term have been derived in Lemma 1.
- Since $\mathbf{h}_{u,\ell} \sim \mathcal{CN}(0, 1)$, we have $\|\mathbf{h}_u\|^2 \propto \chi^2(2L)$. Thus, $\mathbb{E} \{ \|\mathbf{h}_u\|^2 \} = L$ and $\text{Var} \{ \|\mathbf{h}_u\|^2 \} = L$.

Combining the all the means and variances above, the approximated Gaussian distribution of $Z_{n,u}$ as a PP can be obtained as in Lemma 2 according to the central limit theorem [26]. ■

APPENDIX C PROOF OF COROLLARY 1

This proof shows how the pdf of $Z_{n,u}$ can be derived when its first p elements are PPs. The proof for the case when the last p elements of $Z_{n,u}$ are PPs can be done similarly.

First, in terms of the mean vector μ_p of $Z_{n,u}$, it can be easily seen that when the first p elements are PP, the mean value is $M/2$ according to Lemma 2, which means that $\mu_{p,i} = M/2$ for $i \leq p$. Whereas, the remaining elements, which are noise, have zero mean.

In terms of the covariance matrix Σ_p , first, the elements on the main diagonal is the variance of each individual elements of $Z_{n,u}$. Thus, for the first p elements on the main diagonal of Σ_p , which correspond to the p first PPs, $\Sigma_{p,i,i} = \sigma_{\text{PP}}^2$ for $i \leq p$. The remaining elements on the main diagonal Σ_p are the variance of noise, which is $\Sigma_{p,i,i} = \sigma_n^2$ for $i > p$.

The elements on the anti-diagonal of Σ_p is the covariance between two different elements of $Z_{n,u}$, without the loss of generality, say $Z_{n,u}$ and $Z_{n-M,u}$. There are three cases:

- If $Z_{n,u}$ and $Z_{n-M,u}$ are two PPs, they are correlated due to the common term $M\|\mathbf{h}_u\|^2/2L$ as can be seen from (50), while other terms are uncorrelated. Thus, it can be found that $\text{cov} \{ Z_{n,u}, Z_{n-M,u} \} = \mathbb{E} \left\{ \frac{M\|\mathbf{h}_u\|^2}{2L} \right\} = \frac{M^2}{4L}$.
- If either one of $Z_{n,u}$ and $Z_{n-M,u}$ is a PP, while the other is noise, they are uncorrelated, and hence, $\text{cov} \{ Z_{n,u}, Z_{n-M,u} \} = 0$.
- If both $Z_{n,u}$ and $Z_{n-M,u}$ are noise, they are uncorrelated, and hence, $\text{cov} \{ Z_{n,u}, Z_{n-M,u} \} = 0$.

From these cases, the elements on the anti diagonal of the covariance matrix Σ_p can be obtained as in Corollary 1. ■

REFERENCES

- [1] C. Milarokostas, D. Tsolkas, N. Passas and L. Merakos, "A comprehensive study on LPWANs with a focus on the potential of LoRa/LoRaWAN systems," *IEEE Commun. Surv. & Tut.*, vol. 25, no. 1, pp. 825–867, First quarter, 2023.
- [2] A. Maleki, H. H. Nguyen, E. Bedeer and R. Barton, "A tutorial on chirp spread spectrum modulation for LoRaWAN: Basics and key advances," *IEEE Open J. Commun. Soc.*, vol. 5, pp. 4578–4612, 2024.
- [3] X. Wang, L. Kong, L. He and G. Chen, "mLoRa: A multi-packet reception protocol in LoRa networks," in *Proc. IEEE Int. Conf. Netw. Protocols (ICNP)*, Chicago, IL, USA, 2019, pp. 1–11.
- [4] J. Tapparel et. al., "Enhancing the reliability of dense LoRaWAN networks with multi-user receivers," *IEEE Open J. Commun. Soc.*, vol. 2, pp. 2725–2738, 2021.
- [5] K. AlHamdani et. al., "Analysis of superimposed LoRa in multi-user networks," in *Proc. Int. Conf. Adv. Commun. Technol. (CommNet)*, Rabat, Morocco, 2021, pp. 1–6.
- [6] A. Petroni and M. Biagi, "Interference mitigation and decoding through gateway diversity in LoRaWAN," *IEEE Trans. Wireless Commun.*, vol. 21, no. 11, pp. 9068–9081, Nov. 2022.
- [7] M. Xhonneux et. al., "A maximum-likelihood-based two-user receiver for LoRa chirp spread-spectrum modulation," *IEEE Internet Things J.*, vol. 9, no. 22, pp. 22993–23007, Nov. 2022.
- [8] AN1200.86: *LoRa and LoRaWAN*, SemTech, Camarillo, CA, USA, Mar. 2024.
- [9] T. K. Nguyen, H. H. Nguyen and E. Bedeer, "Concurrent transmission and multiuser detection of LoRa signals," *IEEE Internet Things J.*, vol. 10, no. 1, pp. 774–786, Jan. 2023.
- [10] S. Jha and N. M. Balasubramanya, "Multi-user detection and data association for LoRa-based UAV IoT networks," in *Proc. IEEE Global Comm. Conf. Workshops*, Rio de Janeiro, Brazil, 2022, pp. 1170–1175.
- [11] K. Nguyen and E. Bedeer, "Preamble-based successive channel estimation for multiuser massive MIMO LoRaWAN with asynchronous packets," in *Proc. IEEE Veh. Technol. Conf. (VTC-Fall)*, Chengdu, China, Oct. 2025.
- [12] J. Ortín, M. Cesana and A. Redondi, "Augmenting LoRaWAN performance with listen before talk," *IEEE Trans. Wireless Commun.*, vol. 18, no. 6, pp. 3113–3128, Jun. 2019.
- [13] T. K. Nguyen, H. H. Nguyen, and E. Bedeer, "Performance improvement of LoRa modulation with signal combining and semi-coherent detection," *IEEE Commun. Lett.*, vol. 25, pp. 2889–2893, Sep. 2021.
- [14] K. Nguyen, H. H. Nguyen and E. Salt, "Iterative semi-coherent receiver for coded LoRa Systems," *IEEE Commun. Lett.*, vol. 27, no. 3, pp. 971–975, Mar. 2023.
- [15] J. -M. Kang, "On the LoRa modulation for IoT: Preamble designs for channel estimation with single-and multi-chirp transmission strategies," *IEEE Internet Things J.*, vol. 11, no. 17, pp. 27981–27993, Sep. 2024.
- [16] R. Ghanaatian, O. Afisiadis, M. Cotting and A. Burg, "LoRa digital receiver analysis and implementation," in *Proc. IEEE Int. Conf. Acoustics, Speech and Signal Process. (ICASSP)*, Brighton, UK, 2019, pp. 1498–1502.
- [17] P. Edward et. al., "Enhancing the capture capabilities of LoRa receivers," in *Proc. Int. Conf. Smart Appl. Commun. and Network. (SmartNets)*, Sharm El Sheikh, Egypt, 2019, pp. 1–6.
- [18] X. Tang et. al., "Performance analysis of preamble detection of LoRa system," in *Proc. Int. Conf. Electronic Engineering and Informatics (EEI)*, Nanjing, China, 2019, pp. 175–180.
- [19] C. Bernier, F. Dehmas and N. Deparis, "Low complexity LoRa frame synchronization for ultra-low power software-defined radios," *IEEE Trans. Commun.*, vol. 68, no. 5, pp. 3140–3152, May 2020.
- [20] J. -M. Kang, D. -W. Lim and K. -M. Kang, "On the LoRa modulation for IoT: Optimal preamble detection and its performance analysis," *IEEE Internet Things J.*, vol. 9, no. 7, pp. 4973–4986, Apr. 2022.
- [21] J. Tapparel, A. Balatsoukas-Stimming and A. Burg, "LoRa preamble detection robust to inter-channel interference," in *Proc. IEEE Int. Workshop Signal Process. Advances Wireless Commun. (SPAWC)*, Shanghai, China, 2023, pp. 516–520.
- [22] J. -M. Kang, "LoRa preamble detection with optimized thresholds," *IEEE Internet Things J.*, vol. 10, no. 7, pp. 6525–6526, Apr. 2023.
- [23] L. Wang, M. M. Wang and J. Zhang, "Preamble detection performance of LoRa under low-complexity receiver," *IEEE Wireless Commun. Lett.*, vol. 13, no. 9, pp. 2357–2361, Sep. 2024.
- [24] L. Vangelista and A. Cattapan, "Start of packet detection and synchronization for LoraWAN modulated signals," *IEEE Trans. Wireless Commun.*, vol. 21, no. 6, pp. 4608–4621, Jun. 2022.

- [25] T. L. Marzetta, E. G. Larsson, H. Yang, H. Q. Ngo, *Fundamentals of Massive MIMO*. Cambridge University Press, 2016.
- [26] P. Billingsley, *Probability and Measure*, 3rd ed., New York, NY, USA: John Wiley & Sons, 2005.